BMSM

Bulletin of Materials Science & Metallurgy

Periodical Scientific Journal of UCTEA Chamber of Metallurgical and Materials Engineers

Volume 1, Issue 2, 2024, Pages 1-10 Received: 21 March 2024 Accepted: 29 May 2024

Research Article

Effect Of Heat Input On Microstructure And Mechanical Properties Of Tig Welded Aisi 318ln Stainless Steel Plates

Muhammed M. Arslan[a,*], Gürel Çam[b,*]

[a]Iskenderun Technical University, Institute of Engineering and Sciences, Iskenderun-Hatay, Türkiye

[b]Iskenderun Technical University, Faculty of Engineering and natural Sciences, Department of Mechanical Engineering, Iskenderun-Hatay, Türkiye

*Corresponding author's email: gurel.cam@iste.edu.tr

Abstract

Duplex stainless steel is the type with the best corrosion resistance among all types of stainless steel. However, their cost is higher than other stainless steels. Therefore, it is more widely used in areas where the risk of corrosion is high. Therefore, the most common use of duplex stainless steel is in the petrochemical industry. In this sector, where chemicals with high abrasive power are used, duplex stainless steel is used for both the transport and storage of chemicals. Welding is an indispensable fabrication method in these applications. Therefore, there is a need for reliable welding procedures that will not adversely affect the mechanical properties and corrosion behavior of these steels in the weld zone.

In this study, the microstructural evolution and mechanical properties of the 3 mm thick SAF 2205 (AISI 318LN) duplex stainless steel welded joints fabricated by the gas tungsten arc welding method using an ER2209 filler wire were investigated. The microstructures formed in the weld area were examined in detail with an optical microscope. The mechanical properties and welding performance values of the joints obtained were determined by tensile test and microhardness measurements. In addition, the effect of heat input on the microstructure and mechanical properties of welded joints was also investigated.

Keywords

SAF 2205, AISI 318N, TIG, Duplex Stainless Steel, Microstructural Evolution, Weld Performance

1. Introduction

Duplex stainless-steel plates are generally produced by cold rolling in the final stage. Thanks to the ferrite/austenite balance in the microstructure of duplex stainless steels, these materials show high mechanical properties [1-4]. The most important advantage of these steels compared to austenitic stainless steels is that their yield strength is twice as high. In addition, these steels have superior corrosion resistance (high resistance to stress corrosion cracking and pitting corrosion) compared to austenitic stainless steels [3,4]. For this reason, duplex stainless steels, like other stainless steels, are widely used in nuclear facilities, oil and natural gas pipelines (including undersea pipes), offshore platforms, the paper industry, purification facilities, chemical facilities, and maritime (shipbuilding) areas [5-19]. In many of these applications, welding of duplex stainless steel is inevitable.

The weldability of duplex stainless steels is generally better than ferritic stainless steels but worse than austenitic stainless steels. Weld seams of these alloys provide the desired level of mechanical strength and corrosion resistance in most applications, even without being subjected to any heat treatment. The weld nugget microstructure is completely ferritic when it solidifies, but during cooling, some of the ferrite transforms into austenite and the microstructure of the weld nugget becomes duplex. To ensure adequate austenite formation in the heat-affected zone (HAZ), rapid cooling should be avoided. The high heat input and subsequent rapid cooling during the welding process can cause microstructural changes and/or precipitations that negatively affect the properties of the weld seam. Important factors affecting the cooling rate are heat input, minimum and maximum welding parameters specified in the welding procedure, and preheat and interpass temperatures. In a normal welding application, it is

difficult for 475°C brittleness to occur as sigma (σ) phase formation temperatures are passed quickly.

The heat the material is exposed to during the welding process can change the ferrite and austenite ratio of the weld metal and HAZ. The change in this ratio causes the mechanical properties and corrosion resistance of the material to diminish. Therefore, the welding method, welding procedure, and filler wire must be selected to balance this ratio and prevent the formation of harmful phases such as nitrides, carbides, and intermetallics [20]. For example; nitrogen (N) is added to the base material to ensure the easy formation of austenite in the HAZ region adjacent to the fusion zone which is subjected to high temperatures. In addition, to increase the austenite that provides the necessary ductility and toughness in the weld metal, filler wires containing 2-3% more Ni than the Ni content of the base metal are used [21]. It is preferred to use duplex stainless steel filler wire such as ER2209 when welding duplex stainless steels and welding these steels with austenitic stainless steels and carbon or low alloy steels. In some applications, austenitic stainless steel filler wires such as 309L and 309LMo may be recommended, but these lead to a decrease in N content and an increase in the ferritic structure in the HAZ exposed to high temperatures [22]. As in structural steels and other stainless steels [7-18], the most commonly used welding methods in the joining of duplex stainless steels are shielded metal arc welding (SMAW), gas metal arc welding (GMAW), gas tungsten arc welding (GTAW), submerged arc welding (SAW), and flux-cored wire arc welding (FCAW) methods. These high arc energy methods lead to more austenite formation in the weld seam due to the lower cooling rates in these methods [23,24]. On the other hand, high energy density and therefore lower heat input plasma arc welding (PAW), laser beam welding (LBW), and electron beam welding (EBW) methods are also used in the welding of these steels [25-28]. However, lower amounts of austenite form in the weld nugget in these methods as a result of higher cooling rates involved [29,30]. In addition, intensive studies have recently been carried out on the use of new and advanced welding technologies to join duplex steels using appropriate additional wire and welding parameters. Among these, friction stir welding (FSW) [30-40], which was developed to join low melting point metals and alloys such as Al-alloys, active flux gas tungsten arc welding (A-TIG) and hybrid welding techniques (such as hybrid plasma arc-GMAW, hybrid plasma arc-GTAW, hybrid laser-GMAW, and hybrid laser-GTAW) have been investigated [13,23,42-52].

Heat input significantly affects the changes in the microstructure (austenite-ferrite balance) in the weld zone of duplex stainless steel welded joints. In general, a heat input between 0.5-2.0 kJ/mm is recommended to obtain appropriate austenite and ferrite ratios in these steels and to control harmful intermetallic phases [53]. In fact, Hertzman [54] reported that the strength of SAF 2205 duplex stainless steel connections did not change significantly when a heat input of 0.3–2.0 kJ/mm was used or when the amount of ferrite in the weld seam was between 23-53%. Additionally, heat input has a significant impact on the nugget form and the metallurgical, mechanical, and corrosion properties of the welded joint [46]. Therefore, the cooling rate, which varies depending on the heat input and welding method, also plays an important role in the grain size and phase formation in the weld zone [55]. As is clear from the literature, low heat input and rapid cooling lead to the formation of harmful Cr_2N and CrN phases, so they should be avoided.

The GTAW method is one of the most popular welding methods for welding duplex stainless steel. However, the low efficiency of this method limits its widespread use [21,56-59]. For example, Zhang et al. [56] joined 14 mm thick UNS S31803 duplex stainless-steel plates with GTAW and flux-cored wire arc welding (FCAW) using two different shielding gases, pure argon, and argon with 2% nitrogen content and compared the results. A microstructure consisting of ferrite phase, grain boundary austenite, and Widmanstatten austenite was formed in the weld seam of the joints obtained by the GTAW method using both pure argon and nitrogen-doped argon shielding gas. However, the ferrite phase is much less in the weld seam obtained with nitrogen-doped shielding gas. On the other hand, a microstructure containing ferrite phase, intragranular austenite, and grain boundary austenite was formed in the weld nugget of the joints produced by flux-cored wire arc welding. In addition to these phases, inclusions were also detected in the weld zone. Additionally, it has been reported that the addition of nitrogen to the shielding gas in the GTAW process increases the toughness and that joints obtained with flux-cored wire show lower toughness in both the HAZ and the fusion zone. It is also worth pointing out that it is a well-known phenomenon that the formation of the Widmanstatten ferrite in the weld region of structural steels reduces the impact strength [58,59].

Low heat input welding methods (e.g., EBW, PAW, and LBW) offer many advantages in fusion joining of duplex stainless steels, as in all metallic materials, such as low distortion and residual stress formation, very narrow HAZ formation or no significant HAZ formation, high welding speeds, the possibility of welding thick plates, and high efficiency. However, since these methods inherently lead to high cooling rates, this causes excessive ferrite formation in the weld seam as there is not enough time for the solidified ferrite phase to transform into austenite, thus deteriorating the austenite-ferrite balance [28,60-64]. This necessitates heat treatment to ensure ferrite/austenite balance in the fusion zone after welding. Another way to partially preserve the ferrite-austenite balance in the weld region is to use pure nitrogen shielding gas instead of argon shielding gas in the laser

welding process [64]. In addition, since vacuum is used in electron welding, nitrogen loss also occurs, and this negatively affects corrosion resistance as well as mechanical properties [28]. Both high energy density methods such as LBW and EBW and hybrid welding applications are not widely used methods in welding duplex stainless steels. Additionally, these methods require large investment costs. Similarly, the solid-state FSW process, which provides successful results in low-melting alloys such as Al-alloys, also has some disadvantages. This method requires high-cost stirring tools resistant to high temperatures and tight fixing of the plates to be welded before welding and has geometric limitations. Additionally, low cooling rates may lead to negative changes in the microstructure. Additionally, welding speeds in this method are lower than traditional fusion welding processes.

Another method that can be used for welding thick sheets is the active flux GTAW (A-TIG) method. With this method, deep penetration welds can also be obtained in duplex stainless steels. For example, in their study, Zou et al. [49] successfully joined SUS329J4L duplex stainless-steel plates with relatively low heat input A-TIG welding. It has been reported that the microstructure in the fusion zone consists of the ferrite phase, grain boundary austenite (intergranular austenite), and austenite formed within the grains (intragranular austenite). However, this method is not a commonly used welding method for welding duplex stainless steel plates. Additionally, Ravichandran et al. [65] used S/N ratio and ANOVA techniques to determine the optimum welding parameters (such as current, gas flow rate, and welding speed) for welding duplex stainless steels with the GTAW method. S/N analysis results reported that the highest impact resistance and hardness values were obtained at 150 A current, 14 L/min gas flow rate, and 210 mm/min welding speed. Naik and Reddy [66] also TIG welded 6 mm thick 2205 duplex stainless steel plates using ER316 wire and reported that the best results were obtained with a current of 250 A.

As can be understood from the above discussion, there is a need for a detailed understanding of issues such as the effect of heat input in the welding of these steels with low-cost conventional arc welding methods and the development of reliable conventional welding procedures for joining these steels. Therefore, in this study, 3 mm thick SAF 2205 duplex stainless steel plates were butt-welded using a 2 mm diameter ER2209 duplex filler wire in 2 passes with the GTAW method using different heat inputs. To characterize the microstructures formed in the weld region of the fabricated welded joints, detailed microstructural examinations and microhardness measurements were carried out using an optical microscope on the metallography samples cut from the welded joints. Samples extracted from both the base material and the welded joints were subjected to tensile testing to determine the mechanical properties and welding performance. In addition, the effects of heat input on the microstructural changes in the weld region and the performance of the welded joints under tensile and bending conditions were examined.

2. Materials and Methods

In this study, the weldability of 3 mm thick cold-rolled AISI 318LN type duplex stainless steel (SAF 2205 - material number 1.4462) plates with the GTAW method and the effect of heat input on the welding performance were investigated. The chemical compositions of the plates and filler wire used are given in Table 1.

Table 1. Compositions of base plate and filler wire (wt.%)

Chemical composition (wt. %)								
Material	C	Si	Mn	Cr	Ni	Mo	Cu	N
BM*	0,016	0,37	1,49	22,2	5,7	3,1	0,25	0,185
Filler wire	0,01	0,45	1,45	23,0	8,5	--	--	0,15

*In addition, BM also contains % 0,017 Nb, % 0, 18 Co, % 0,026 P, and % 0,001 S.

For welding experiments, rectangular pieces 195x300 mm in size were cut from the commercially available plate perpendicular to the rolling direction, and the weld grooves were machined in these parts as shown in Figure 1. The surfaces were mechanically cleaned with a stainless-steel brush before the joining process. Welding trials were carried out in two passes, namely root pass and filler pass, using a 2 mm diameter duplex filler wire (ER2209) at different heat inputs. During the welding process, filler wire was fed at a speed of 1.5 mm/s in each pass. In all welding experiments, 99.95% purity argon gas was supplied to the welding area as a protective gas at a flow rate of 16 L/min. In all welds, a ceramic backing was used to prevent underfill failure as a result of liquid metal flowing from the weld base. Additionally, the chassis connection and extension cable were kept in a straight position during the welding process. Other welding parameters used in the welding process are given in Table 2.

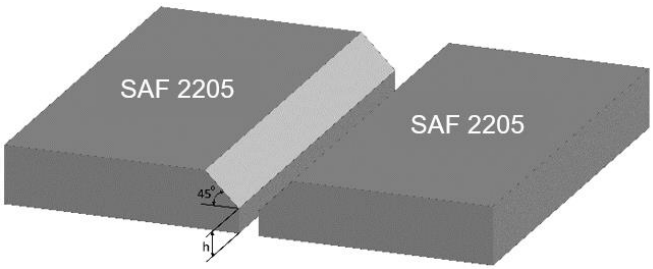

Figure 1. Preparation of plates for welding (h: 1 mm, the gap between the plates at weld root: 2 mm).

One metallography sample, two bending samples, and four tensile samples were extracted from each welded joint obtained to determine the microstructural changes occurring in

the weld region and to evaluate the effect of the changes in the microstructure on the mechanical properties. For comparison purposes and to evaluate joint performance, at least three tensile specimens were also prepared from the base plate according to ASTM A370 standards. To examine the weld cross-section following grinding and polishing, metallography samples were etched for 20 seconds using a solution consisting of 50 ml HCl and 150 ml HNO3 (aqua regia). In addition to microhardness measurements, detailed microstructure examinations were also carried out on the metallography samples. As shown schematically in Figure 2, microhardness measurements were made on the metallography samples on a line around the centre of the weld cross-section, using a load of 980 N (10 kg) in all regions in the samples, namely in the base plates, HAZs, and FZs. With these measurement values, the hardness distribution (hardness profile) along the weld cross-section was determined for each welded joint.

Table 2. Weld parameters used in welding trials.

Welding Procedure	Current (A)	Voltage (V)	Weld Speed (mm/min)	Heat Input (kJ/mm)
Low Heat Input*	120	28	36	3,92
Medium Heat Input*	130	28	36	4,25
High Heat Input*	140	28	36	4,57

Heat input was calculated using the following equation: $q = \eta I U 60/1000 v$ (q = heat input (kJ/mm), η = arc efficiency (for GTAW it is 0,7), U = arc voltage (V), I = current (A), and v = weld speed (mm/min)).

Additionally, to determine the mechanical properties, mechanical performances, and joint qualities of welded plates, tensile test specimens extracted from both the base plate and welded joints were tested with a deformation rate of 0.0025 1/s according to ISO 6892-1. Two bending samples were also extracted from each welded joint to determine whether there was any cracking under bending conditions in the weld region of the joints produced. One of these bending specimens was bent in the face-bending condition and the other in the root-bending configuration. The bending samples were bent to approximately 140-150 degrees with the weld centre in the middle position.

3. Results and Discussion

The findings obtained in this study will be discussed under two subheadings in this section.

3.1. Microstructural Aspects

The microstructure of the 3 mm thick SAF 2205 duplex stainless steel base plate used in this study is given in Figure 3. As can be seen from the figure, the base plate has a microstructure consisting of austenite (50%) and delta ferrite (50%). Owing to the ferrite/austenite balance in this microstructure, these steels exhibit high mechanical properties and at the same time superior corrosion resistance (higher resistance to stress corrosion cracking and pitting corrosion) compared to austenitic stainless steels.

Duplex stainless steels solidify completely in ferritic mode, and austenite solid nuclei are formed in the ferrite phase under the ferrite solidification curve (the solidification sequence is as follows: Liquid → Liquid + δ → δ + γ), resulting in a microstructure consisting of ferrite and austenite. This solidification mode depends on the Cr_{eq}/Ni_{eq} ratio and can be better understood from the Fe-Cr-Ni phase diagram given in Figure 4, which is a very good reference for understanding the solidification mode [56,67,68].

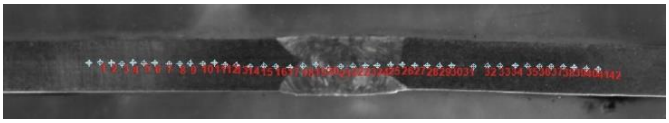

Figure 2. Macrograph showing the points where microhardness measurements were made in the weld cross-section.

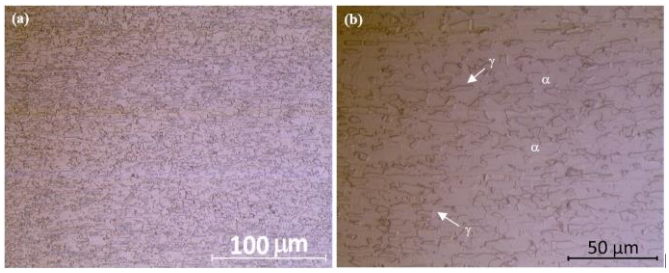

Figure 3. Microstructure of the duplex stainless steel base plate used in the study: (a) 200X and (b) 500X magnification.

The composition of typical duplex stainless steels corresponds to the α + γ phase region. Duplex stainless steels such as SAF 2205 and SAF 2507 are marked in Figure 4. As can be seen from this figure, the ferrite phase is constantly present from solidification down to room temperature, and therefore, although it is delta (δ) ferrite, it is called alpha (α) ferrite because it transforms with the same chemical composition [69].

In practice, duplex stainless steels are resistant to solidification cracking because they contain low impurity. If the Cr_{eq}/Ni_{eq} ratio is greater than 1.95, the solidification in stainless steels is completely ferritic. However, if this ratio is between 2.25-3.5 (for SAF 2205, this ratio is 2.62), the solidification is two-phase (ferrite + austenite). In general, a microstructure consisting of a ferrite matrix containing grain boundary austenite (GBA) nucleated within the ferrite matrix and Widmanstatten austenite (WA) is observed in the fusion zone of duplex stainless steels [70]. Later, with the effect of the

cooling rate, an intragranular austenite phase (IGA) is also formed, which requires more driving force at lower temperatures and is sensitive to pitting corrosion.

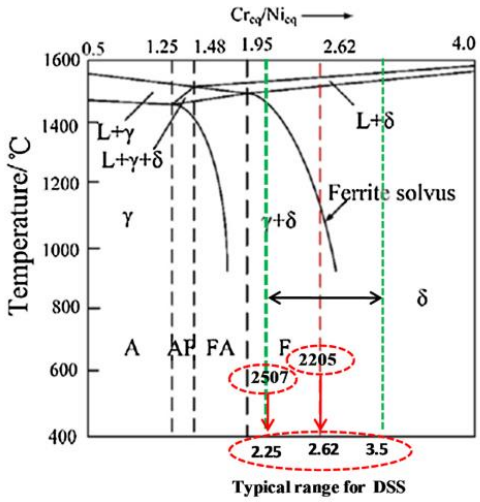

Figure 4. Fe-Cr-Ni diagram showing the types of solidification occurring in stainless steels depending on the Cr_{eq}/Ni_{eq} ratio (solidification of SAF 2205 duplex stainless steel is also marked in the diagram).

Figure 5 gives macrographs showing the weld cross-sections of the welded joints obtained in this study. As can be seen from these macrographs, the weld profiles of the joints are quite good and no weld defects such as porosity, cracks, etc. were observed in the weld regions, except the low heat input joint. This indicates that the joint quality of the welded plates is satisfactory. However, a decrease in cross-section was observed in the joint obtained with low heat input as a result of insufficient filling. The microstructure formed in the fusion zone of the joint produced with low heat input (3.92 kJ/mm) is shown in Figure 6. As can be seen from the figure, the microstructure contains a ferrite phase containing grain boundary austenite, a small amount of Widmanstatten austenite, and intragranular austenite. Additionally, another noteworthy point is that the amount of ferrite in the fusion zone of this joint is higher than the austenite content.

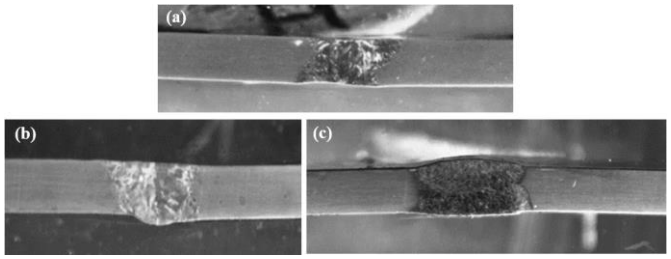

Figure 5. Macrographs showing the cross-section of the welded joints: The welded joint produced with a heat input of: (a) 3.92, (b) 4.25 and (c) 4.57 kJ/mm. (thickness: 3mm).

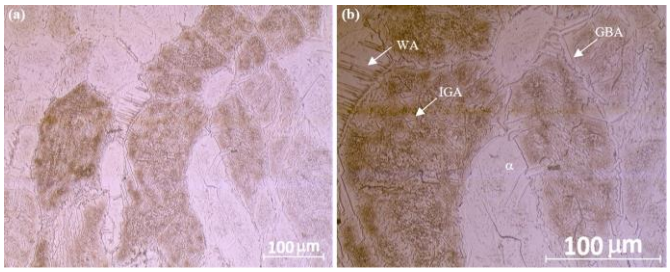

Figure 6. Microstructure in the FZ of low-heat input joint (3.92 kJ/mm): (a) X100 and (b) X200 magnification. (GBA: Grain boundary austenite, IGA: Intragranular austenite and WA: Widmanstten austenite).

As an example of the fusion zone microstructures of joints made with medium (4.25 kJ/mm) and high (4.57 kJ/mm) heat inputs, the microstructure observed in the fusion zone of the joint with high-heat input is given in Figure 7. As can be seen from the figure, the fusion zone microstructure of these joints comprises a ferrite phase containing grain boundary austenite, a small amount of Widmanstatten austenite, and intragranular austenite, similar to the joint produced with low heat input. However, the amount of Widmanstatten austenite and intragranular austenite is higher. In addition, while a finer-grained equiaxed structure forms in the fusion zone of the joint produced with low heat input, it is observed that a coarse-grained, columnar grain structure forms in the fusion of the joints obtained with medium and high heat inputs. This columnar grain structure is more evident in the joint made with high heat input (4.57 kJ/mm) (Figure 7b). In addition, in the fusion zones of joints produced with medium and high heat input, especially in that of the high-heat input, the amount of austenite is much higher than in the low-heat input joint, and the ferrite-austenite balance is better.

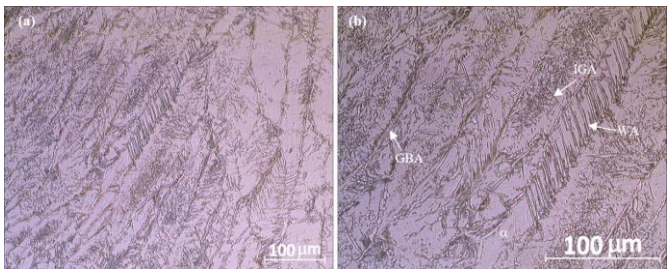

Figure 7. Microstructure in the FZ of high-heat input joint (4,57 kJ/mm): (a) X100 and (b) X200 magnification. (GBA: Grain boundary austenite, IGA: Intragranular austenite and WA: Widmanstten austenite).

As an example of welded joints produced with 3.92 and 4.25 kJ/mm heat inputs, optical micrographs showing the microstructure of the heat-affected zone (HAZ) of the joint produced with medium-heat input (4.25 kJ/mm) are given in Figure 8. As can be seen from the figure, no visible HAZ was present in both joints. On the other hand, it was observed that an evident HAZ occurred in the welded joint obtained with high heat input (4.57 kJ/mm). As clearly seen from Figure 9,

recrystallization took place in the HAZ of this joint. The temperatures reached during welding in this region are at a level that will lead to the formation of the ferrite phase. Therefore, as a result of the recrystallization in the HAZ of this joint, a relatively coarse-grained ferritic structure was formed due to the relatively high heat input. Moreover, due to the relatively rapid cooling after welding, the formation of the austenite phase within the ferrite phase was limited. As a result, the microstructure in the HAZ of this joint consists of coarse ferrite grains and a small amount of grain boundary austenite and intragranular austenite (austenite phase formed within the grains). In addition, the ferrite phase present in the microstructure is more than the austenite phase, due to the relatively rapid cooling after welding and thus the limited formation of the austenite phase within the ferrite phase.

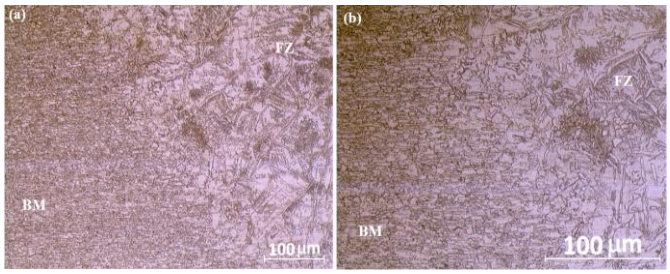

Figure 8. Microstructure in the HAZ of medium-heat input joint (4,25 kJ/mm): (a) X100 and (b) X200 magnification. (BM: Base metal and FZ: Fuzion zone).

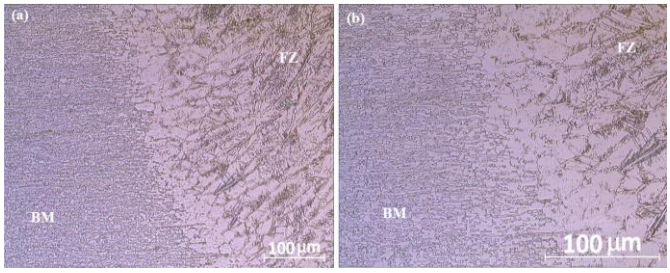

Figure 9. Microstructure in the HAZ of high-heat input joint (4,57 kJ/mm): (a) X100 and (b) X200 magnification. (BM: Base metal and FZ: Fuzion zone).

3.2. Mechanical Properties

3.2.1. Microhardness

The hardness profiles showing the hardness distribution along the weld cross-sections of all the joints drawn using the hardness values obtained by microhardness measurements taken at the points shown in Figure 2 are given in Figure 10. As seen from the figure, the hardness profile of the low-heat input joint (3.92 kJ/mm), which exhibited an increase in hardness in the weld region, is different from those of the other joints (medium and high heat inputs). This indicates that the ferrite-austenite ratio in the fusion zone of this joint is negatively affected and is related to the increase in the amount of ferrite as a result of less austenite formation due to rapid cooling. These results are in good agreement with the microstructural observations.

On the other hand, no hardness increase was observed in the weld regions of the joints produced using medium and high heat inputs (4.25 and 4.57 kJ/mm), and hardness values similar to the hardness value of the base material were measured. Therefore, while the low-heat input joint displayed an increase in strength (strength overmatching) in the weld region, the joints produced with medium and high heat inputs exhibited a homogeneous hardness distribution throughout the weld cross-section (strength even matching weld region). These results are due to the preservation of the ferrite-austenite balance in these two joints, especially in the high-heat input joint, and are compatible with the microstructural investigations. In addition, although coarse ferrite grains and grain boundary austenite are formed in the very narrow HAZ exposed to high heat adjacent to the fusion line of the high heat input joint, no change variation (hardness decrease) in the hardness profile was observed. This is attributed to the fact that this region is very narrow and as a result, no hardness measurement could be made in this region.

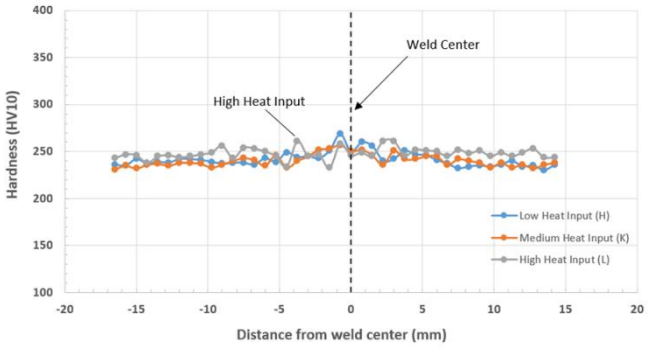

Figure 10. Hardness profiles of the joints obtained with different heat inputs.

3.2.2. Tensile and Bending Performance

The tensile test results obtained from the base plate samples and the samples extracted from the joints perpendicular to the weld line are summarized in Table 3. As can be seen in Figure 11, all the specimens extracted from the low-heat input joint fractured within the weld region. On the other hand, two of the tensile samples of the medium-heat input joint broke within the FZ and the other two failed within the base plate at a certain distance from the HAZ. While only one of the samples of the high-heat input joint broke off from the weld region, the other three samples fractured in the base metal close to the HAZ. These results are also compatible with the microstructural examinations. It is caused by the deterioration of the ferrite-austenite phase balance in the FZ of the low-heat input joint along with a significant thinning in the weld cross-section in this joint due to insufficient filling, as seen from the macrograph of this joint in Fig. 5(a). Additionally, as seen from the table, the tensile strength of the samples of the low-

heat input joint is lower those that of base plate samples, and the joint performance value in terms of strength is 96%. The strength levels of medium and high-heat input joint samples, particularly that of high-heat input joint, are higher than those of the low-heat input joint and the base plate samples, thus the strength performance is around 102%. This situation is clearly seen from the stress-strain curves obtained from the base plate and welded joint samples given in Figure 12. The reason why the high-heat input joint exhibits high strength performance is the result of better preservation of the ferrite-austenite balance in the fusion zone of this joint (Figure 7b).

Table 3. Tensile test results (average values are given in parentheses).

Specimen	R_m (MPa)	Elongation (%)	Strength Performance (%)	Ductility Performance (%)
Base Metal	807; 811; 809; 806 (**808**)	26; 26; 26; 25 (**26**)	--	--
Low Heat Input Joint	757; 760; 777; 799 (**773**)	9; 7; 9; 13 (**10**)	96	38
Medium Heat Input Joint	826; 821; 745; 759 (**788**)	22; 22; 7; 9 (**15**)	98	58
High Heat Input Joint	833; 831; 816; 831 (**828**)	25; 21; 22; 23 (**23**)	102	88

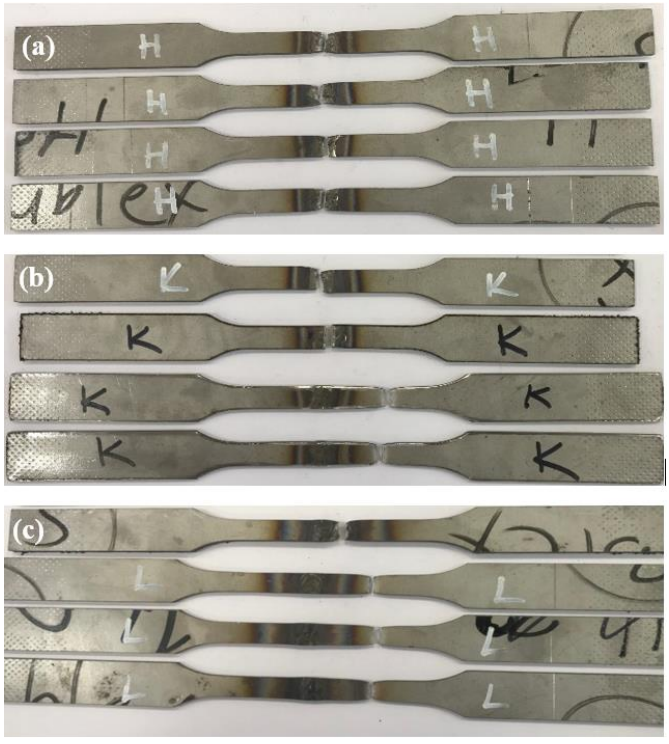

Figure 11. Fracture locations in tensile samples of the welded joints: (a) Low, (b) medium, and (c) high heat input joints.

On the other hand, as seen in Table 3, the elongation values of the welded joint samples are significantly lower than the base plate. This is due to the inhomogeneity of the welded joint samples. This situation is especially evident in the low-heat input joint, and the joint performance in terms of ductility is quite low (38%). The reason for this is that in these samples, where the fracture occurs in the FZ, no elongation occurs in the base plate, and therefore plastic deformation is limited to the weld region (i.e., confined plasticity). The highest ductility performance was displayed by the high-heat input joint (i.e., 88%). This result is consistent with the fact that all but one of the samples broke from the base plate due to better preservation of the ferrite-austenite balance in the FZ of this joint. Similar results are also observed in welded joints with a strength increase in the weld area (strength overmatching joints) [71-74]. Moreover, generally, much lower ductility performance values have been reported in high-strength Al-alloy welded joints with excessive strength loss in the weld region (highly strength undermatching joints) where only the weld region undergoes plastic deformation [75-80] as well as in diffusion welded dissimilar joints in which plastic deformation occurs only in the half of the sample [81,82].

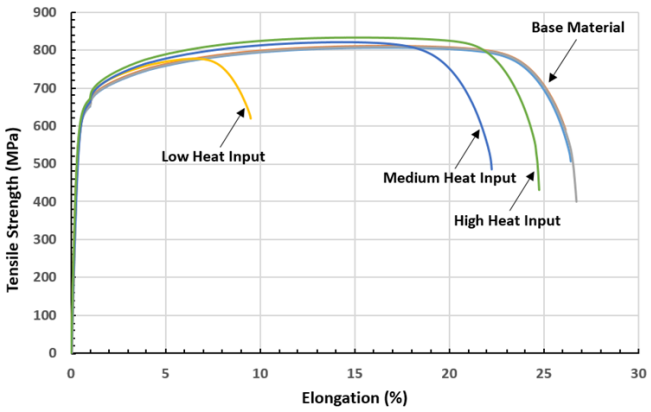

Figure 12. Stress-strain curves obtained from the base plate and welded samples.

In addition, no cracking was observed in any of the samples in both the surface bending and root bending tests performed on all welded joints, indicating that the weld quality was satisfactory. These results are compatible with microstructural observations in which discontinuities such as cracks and porosity are not detected in the weld regions of the joints.

4. Conclusion

In this study, 3 mm thick cold-rolled SAF 2205 duplex stainless steel plates were successfully welded in two passes by the GTAW method using an ER 2209 filler wire with a diameter of 2 mm. The results obtained from this study can be summarized as follows:

- No weld discontinuities such as porosity or crack formation were detected in all the welded joints produced.

- A microstructure comprising of ferrite phase containing grain boundary austenite, a small amount of Widmanstatten austenite, and intragranular austenite was detected in the FZ of the welded joints. While an equiaxed structure was formed in the FZ of the low-heat input joint, coarse columnar grains were observed in the FZ of the medium and high-heat input joints. In addition, the amount of austenite in the FZ was higher in medium and high-heat input joints, especially in the high-heat input joint.
- While no visible HAZ was observed in the low and medium heat-input joint, a distinct HAZ occurred as a result of recrystallization in the high-heat input joint.
- The hardness profile of the low-heat input joint (3.92 kJ/mm) is different from the other joints (medium and high-heat inputs), and an increase in hardness is observed in the weld region of this joint, while the medium and high-heat input joints (4.25 and 4.57 kJ/mm) mm) exhibited a more homogeneous hardness distribution across the weld cross-section.
- All transverse tensile test specimens of the low-heat input joint broke off within the weld region. On the other hand, two of the samples of the medium-heat input joint and only one of the samples of the high-heat input joint fractured within the weld nugget, the other samples failed in the base plate.
- The high-heat input joint showed the highest strength performance value (i.e., 102%). This is the result of better preservation of the ferrite-austenite balance in the FZ of this joint. On the other hand, due to the non-homogeneity of the transverse tensile samples, the ductility performance of all joints is low, and the highest ductility performance (i.e., 88%) was displayed by the high-heat input joint. This indicates that heat input plays an important role on the microstructural evolution in the FZ and thus mechanical performance. Sufficiently higher heat inputs for avoiding fast cooling after the welding give better results.
- No cracking occurred in both the surface and root bending samples extracted from all joints. This shows that the heat input range used in the study does not have a significant effect on the joint performance under bending conditions.

Declaration of Competing Interest

The authors declare that they have no known competing financial interests or personal relationships that could have appeared to influence the work reported in this paper.

Acknowledgement

The authors also thank Mr. Sedat UYSAL (Managing Director) and Mr. Tuğrul YAZGAN (Quality and Mechanical Laboratory Supervisor) as well as Mr. Erhan Zeytun and Mr. Ferhat Gürler (Mechanical Laboratory Personnel) from NOKSEL Steel Pipe Inc., İskenderun-Hatay, Turkey, for their valuable support in conducting the metallographic investigations and mechanical tests (tensile and bending tests).

References

[1] T. Oshima, Y. Habara, and K. Kuroda, Efforts to save nickel in austenitic stainless steels, ISIJ Int., 47 (2007) 359-364.

[2] P. Boillot and J. Peultier, Use of stainless steels in the industry: recent and future developments, Procedia Eng., 83 (2014) 309-321.

[3] S.K. Ghosh and S. Mondal, High temperature ageing behaviour of a duplex stainless steel, Mater. Charact., 59 (2008) 1776-1783.

[4] B. Gideon, L. Ward, and G. Biddle, Duplex stainless steel welds and their susceptibility to intergranular corrosion, J. Miner. Mater. Charact. Eng., 7(3)(2008) 247-263.

[5] J. Verma and R.V. Taiwade, Dissimilar welding behavior of 22% Cr series stainless steel with 316L and its corrosion resistance in modified aggressive environment, J. Manuf. Process., 24 (2016) 1-10.

[6] K.D. Ramkumar et al., Studies on the structure–property relationships and corrosion behaviour of the activated flux TIG welding of UNS S32750, J. Manuf. Process., 23 (2016) 231-241.

[7] M. Şenol and G. Çam, Investigation into microstructures and properties of AISI 430 ferritic steel butt joints fabricated by GMAW, Int. J. Press. Ves. Pip., 202 (2023) 104926.

[8] A. Günen et al., A new approach to improve some properties of wire arc additively manufactured stainless steel components: Simultaneous homogenization and boriding, Surface & Coating Technology, 460 (2023) 129395.

[9] U. Gürol et al., Effect of powder-pack aluminizing on microstructure and oxidation resistance of wire arc additively manufactured stainless steels, Surf. Coat. Technol., 468 (2023) 129742.

[10] H.T. Serindağ and G. Çam, Characterizations of microstructure and properties of dissimilar AISI 316L/9Ni low alloy cryogenic steel joints fabricated by GTAW, J. Mater. Eng. Perform., 32 (2023) 7039-7049.

[11] H.T. Serindağ and G. Çam, Multi-pass butt welding of thick AISI 316L plates by gas tungsten arc welding: Microstructural and mechanical characterization, Int. J. Press. Ves. Pip., 200 (2022) 104842.

[12] M. Ezer and G. Çam, A Study on microstructure and mechanical performance of gas metal arc welded AISI 304L joints, Materialwissenschaft und Werkstofftechnik, 53 (9) (2022) 1043-1052.

[13] T. Küçükömeroğlu et al., Investigation of mechanical and microstructural properties of friction stir welded dual phase (DP) steel, IOP Conf. Series: Mater. Sci. Eng., 629 (2019) 012010.

[14] H.T. Serindağ and G. Çam, Microstructural and mechanical characterization of gas tungsten arc welded 10 mm thick AISI 316L joints, Düzce University Journal of Science & Technology, 10 (4) (2022) 1873-1889.

[15] H.T. Serindağ and G. Çam, Microstructure and mechanical properties of gas metal arc welded AISI 430/AISI 304 dissimilar stainless steels butt joints, Journal of Physics: Conference Series, 1777 (2021) 012047.

[16] M. Şenol and G. Cam, Microstructural and mechanical characterization of gas metal arc welded AISI 430 ferritic stainless steel joints, European J. Eng. and Natural Sciences (EJENS), 5 (1) (2020) 52-60.

[17] M. Ezer and G. Çam, Investigation of the microstructure and mechanical properties of gas metal arc welded AISI 304 austenitic stainless steel butt joints, European J. Eng. and Natural Sciences (EJENS), 5 (1) (2020) 43-51.

[18] J.C. Lippold and D.J. Kotecki, 'Welding metallurgy and weldability of stainless steels', John Wiley and Sons, Inc., Hoboken, NJ, USA, (2005) 141-200.

[19] G. Çam, 'Kaynak Bilimi ve Teknolojisi', Nobel Akademik Yayıncılık, Ankara, (2020) 205-209.

[20] L. Karlsson, Welding duplex stainless steels - A review of current recommendations, Weld. World, 56 (2012) 65-76.

[21] S. Geng et al., Evolution of microstructure and corrosion behavior in 2205 duplex stainless steel GTA-welding joint, J. Manuf. Process., 19 (2015) 32-37.

[22] H. Dolutaş and M. Cavcar, 'Dupleks Paslanmaz Çeliklerin Kaynağı', Oerlikon Kaynak Elektrodları ve Sanayi A.Ş., Ankara, (2001) 7-11.

[23] J. Verma and R.V. Taiwade, Effect of welding processes and conditions on the microstructure, mechanical properties and corrosion resistance of duplex stainless steel weldments - A review, J. Manuf. Process., 25 (2017) 134-152.

[24] S.H. Wang et al., Gamma phase transformation in pulsed GTAW weld metal of duplex stainless steel, Mater. Sci. Eng. A, 420 (2006) 26-33.

[25] A.-H.I. Mourad, A. Khourshid, and T. Sharef, Gas tungsten arc and laser beam welding processes effects on duplex stainless steel 2205 properties, Mater. Sci. Eng. A, 549 (2012) 105-113.

[26] E. Taban and E. Kaluc, Welding behaviour of duplex and super-duplex stainless steels using laser and plasma arc welding processes, Weld. World, 55 (2011) 48-57.

[27] S. Krasnorutskyi, D. Keil, S. Schmigalla, M. Zinke, A. Heyn, and H. Pries, Metallurgical investigations on electron beam welded duplex stainless steels, Weld. World, 56 (2012) 34-40.

[28] J.S. Ku, N.J. Ho, and S.C. Tjong, Properties of electron beam welded SAF 2205 duplex stainless steel, J. Mater. Process. Technol., 63 (1997) 770-775.

[29] T. Kannan and N. Murugan, Effect of flux cored arc welding process parameters on duplex stainless steel clad quality, J. Mater. Process. Technol., 176 (2006) 230-239.

[30] J. Nowacki, Ferritic-austenitic steel and its weldability in large size constructions, J. Achiev. Mater. Manuf. Eng., 32 (2) (2009) 115-141.

[31] M.M.Z. Ahmed, et al., Friction stir welding in the aerospace industry: The current progress and state-of-the-art review, Materials, 16 (2023) 2971.

[32] G. Çam, V. Javaheri, and A. Heidarzadeh, Advances in FSW and FSSW of dissimilar Al-alloy plates, Journal of Adhesion Science and Technology, 37 (2) (2023) 162-194.

[33] N. Kashaev, V. Ventzke, and G. Çam G, Prospects of laser beam welding and friction stir welding processes for aluminum airframe structural applications, J. Manuf. Process., 36 (2018) 571-600.

[34] G. Çam and G. İpekoğlu, Recent developments in joining of aluminium alloys, Int. J. Adv. Manuf. Technol., 91 (5-8) (2017) 1851-1866.

[35] G. İpekoğlu et al., Investigation into the effect of temper condition on friction stir weldability of AA6061 Al-alloy plates, Kovove Mater., 51 (3) (2013) 155-163.

[36] G. Çam, Friction stir welded structural materials: Beyond Al-alloys, Int. Mater. Rev., 56 (1) (2011) 1-48.

[37] G. İpekoğlu, Ö. Akçam, and G. Çam, Determination of the suitable weld parameters for friction stir welding of AA6061-T6 plates with different thicknesses, Afyon Kocatepe Univ. J. of Sci. and Eng., 18 (1) (2018) 324-335.

[38] G. Çam, Friction stir welding: A novel welding technique developed for Al-alloys, Mühendis ve Makine, 46 (541) (2005) 30-39.

[39] M.M.Z. Ahmed, et al., A review on friction stir welding of dissimilar Al- and Mg-alloys: Scientometric analysis and strategies for achieving high-quality joints, Journal of Magnesium and Alloys, 11 (2023) 4082-4127.

[40] U.A. Khaliq, et al., A comprehensive review on friction stir welding of aluminum with magnesium: A new insight on joining mechanisms by interfacial enhancement, Journal of Materials Research and Technology (JMR&T), 27 (2023) 4595-4624.

[41] A. Günen et al., Microstructural and mechanical properties of friction stir welded pure lead, Indian J. of Eng. & Mater. Sciences, 25 (1) (2018) 26-32.

[42] H.S. Wang, Effect of welding variables on cooling rate and pitting corrosion resistance in super duplex stainless weldments, Mater Trans., 46 (2005) 593-601.

[43] M.C. Theodoro et al., Dissimilar friction stir welding between UNS S31603 austenitic stainless steel and UNS S32750 superduplex stainless steel, Metall. Mater. Trans. B, 46 (2015) 1440-1447.

[44] T. Saeid et al., Effect of friction stir welding speed on the microstructure and mechanical properties of a duplex stainless steel, Mater. Sci. Eng. A, 496 (2008) 262-268.

[45] R.I. Hsieh, H.Y. Liou, and Y.T. Pan, Effects of cooling time and alloying elements on the microstructure of the gleeble-simulated heat-affected zone of 22% Cr duplex stainless Steels, J. Mater. Eng. Perform., 10 (2001) 526-536.

[46] P.K. Giridharan and N. Murugan, Optimization of pulsed GTA welding process parameters for the welding of AISI 304L stainless steel sheets, Int. J. Adv. Manuf. Technol., 40 (2009) 478-489.

[47] K. Nanda Naik et al., Finite element simulation of A-TIG welding of duplex stainless steel 2205 using SYSWELD, Appl. Mech. Mater., 592-594 (2014) 374-379.

[48] A. Berthier, P. Paillard, and F. Christien, Structural and chemical evolution of super duplex stainless steel on activated tungsten inert gas welding process, Sci. Technol. Weld. Join., 14 (2009) 681-690.

[49] Y. Zou, R. Ueji, and H. Fujii, Mechanical properties of advanced active-TIG welded duplex stainless steel and ferrite steel, Mater. Sci. Eng. A, 620 (2015) 140-148.

[50] E.M. Westin, K. Stelling, and A. Gumenyuk, Single-pass laser-GMA hybrid welding of 13.5 mm thick duplex stainless steel, Weld. World, 55 (2011) 39-49.

[51] E. Taban, Joining of duplex stainless steel by plasma arc, TIG, and plasma Arc + TIG welding processes, Mater. Manuf. Process., 23 (2008) 871-878.

[52] K. Yurtisik et al., Characterization of duplex stainless steel weld metals obtained by hybrid plasma-gas metal arc welding, Soldag Insp., 18 (2013) 207-216.

[53] M. Sadeghian et al., Effect of heat input on microstructure and mechanical properties of dissimilar joints between super duplex stainless steel and high strength low alloy steel, Mater. Des., 60 (2014) 678-684.

[54] S. Hertzman, The influence of nitrogen on microstructure and properties of highly alloyed stainless steel welds, ISIJ Int., 41 (6) (2001) 580-589.

[55] N. Karunakaran, Effect of pulsed current on temperature distribution, weld bead profiles and characteristics of GTA welded stainless steel joints, Int. J. Eng. Technol., 2 (2012) 908-1916.

[56] Z. Zhang et al., Investigation on microstructure evolution and properties of duplex stainless steel joint multi-pass welded by using different methods, Mater. Des., 109 (2016) 670-685.

[57] K. Devendranath et al., Effect of optimal weld parameters in the microstructure and mechanical properties of autogenous gas tungsten arc weldments of super-duplex stainless steel UNS S32750, Mater. Des., 66 (2015) 356-365.

[58] J.C. Jorge, L.F. Souza, and J.M. Rebello, The effect of chromium on the microstructure/toughness relationship of C-Mn weld metal deposits. Materials Characterization, 47 (2001) 195-205.

[59] U. Gürol, O. Çoban, I.C. Coşar, and M. Koçak, Effect of the notch location on the Charpy-V toughness results for robotic flux-cored arc welded multipass joints. Materials Testing, 64 (9) (2022) 1278-1289.

[60] S. Saravanan et al., Pulsed Nd: YAG laser welding and subsequent post-weld heat treatment on super duplex stainless steel, J. Manuf. Process., 25 (2017) 284-289.

[61] A. Pramanik, G. Littlefair, and A.K. Basak, Weldability of duplex stainless steel, Mater. Manuf. Process., 30 (9) (2015) 1053-1068.

[62] E. Capello et al., Laser welding and surface treatment of a 22Cr–5Ni–3Mo duplex stainless steel, Mater. Sci. Eng. A, 351 (1-2) (2003) 334-343.

[63] H.C. Wu, L.W. Tsay, and C. Chen, Laser beam welding of 2205 duplex stainless steel with metal powder additions, ISIJ Int., 44 (10) (2004) 1720-1726.

[64] R. Lai et al., Influence of absorbed nitrogen on microstructure and corrosion resistance of 2205 duplex stainless steel joint processed by fiber laser welding, J. Mater. Process. Technol., 231 (2016) 397-405.

[65] M. Ravichandran et al., Investigation on TIG welding parameters of 2205 duplex stainless steel, Int. J. of Automotive and Mech. Eng., 14 (2017) 4518-4530.

[66] A.B. Naik and A.C. Reddy, Experimental analysis of TIG welding and comparison between activated-TIG and TIG on duplex stainless steel (2205), Int. J. of Scientific & Eng. Res., 7 (6) (2016) 115-122.

[67] Z. Sun et al., Effect of dual torch technique on duplex stainless steel welds, Mater. Sci. Eng. A, 356 (2003) 274-282.

[68] G.L. Leone and H.W. Kerr, The ferrite to austenite transformation in stainless steels. Weld. J., 61 (1982) 13s-22s.

[69] J.W. Fourie and F.P.A. Robinson, Literature review on the influence of weld-heat inputs on the mechanical and corrosion properties of duplex stainless steels, J. S. Afr. Inst. Min. Metall., 90 (1990) 59-65.

[70] H. Sieurin and R. Sandstrom, Austenite reformation in the heat-affected zone of duplex stainless steel 2205, Mater. Sci. Eng. A, 418 (2006) 250-256.

[71] T. Küçükömeroğlu et al., Microstructure and mechanical properties of friction stir welded St52 steel joints, Int. J. Miner. Metall. Mater., 25 (12) (2018) 1457-1464.

[72] G. Çam et al., Investigation into properties of laser welded similar and dissimilar steel joints, Sci. Technol. Weld. Join., 3 (4) (1998) 177-189.

[73] G. Çam et al., Microstructural and mechanical characterization of friction stir butt joint welded 63%Cu-37%Zn brass plate, Weld. J., 88 (11) (2009) 225s-232s.

[74] J. Dos Santos et al., Properties of power beam welded steels, Al- and Ti-alloys: Significance of strength mismatch, Welding in the World, 44 (6) (2000) 42-64.

[75] G. İpekoğlu and G. Çam, Formation of weld defects in cold metal transfer arc welded 7075-T6 plates and its effect on joint performance, IOP Conf. Series: Mater. Sci. Eng., 629 (2019) 012007.

[76] G. İpekoğlu et al., Investigation of the effect of temper condition friction stir weldability of AA7075 Al-alloy plates, Mater. Tehnol., 46 (6) (2012) 627-632.

[77] G. Çam et al., Mechanical properties of friction stir butt-welded Al-5086 H32 plate, Mat.-wiss. u. Werkstofftech., 40 (8) (2009) 638-642.

[78] G. Çam, Prospects of producing aluminum parts by wire arc additive manufacturing (WAAM), Materials Today: Proceedings, 62 (1) (2022) 77-85.

[79] G. Çam, et al., Characterization of laser and electron beam welded Al-alloys, Prakt. Metallogr., 36 (2) (1999) 59-89.

[80] H. Yavuz and G. Çam, A novel welding technique: Friction stir welding, Endüstri ve Otomasyon, 51 (2001) 18-20.

[81] G. Çam et al., Fracture behaviour of diffusion bonded bimaterial Ti-Al joints, Sci. Technol. Weld. Join., 2 (3) (1997) 95-101.

[82] M. Koçak, M. Pakdil, and G. Çam, Fracture behaviour of diffusion bonded Ti-alloys with strength mismatch, Sci. Technol. Weld. Join., 7 (4) (2002) 187-196.